Journal of Materials Chemistry A

Accepted Manuscript

ROYAL SOCIETY OF CHEMISTRY

www.rsc.org/materialsA

Journal Name

ARTICLE

N-type cathode interlayer based on dicyanomethylenated quinacridone derivative for high-performance polymer solar cells

Received 00th January 20xx,
Accepted 00th January 20xx

DOI: 10.1039/x0xx00000x

www.rsc.org/

Weiping Chen, Junjie Lv, Jianxiong Han, Youchun Chen, Tao Jia, Fenghong Li* and Yue Wang*

A new π-conjugated electrolyte bis(dicyanomethylene)-quinacridone with two octyl-pyridium (DCNQA-PyBr) has been synthesized and employed as a solution-processed cathode interlayer (CIL) for polymer solar cells (PSCs). The devices exhibited simultaneously increased open-circuit voltage (V_{oc}), short-circuit current (J_{sc}) and fill factor (FF). Overall, the 13 nm DCNQA-PyBr interlayer inserted PSCs with PCDTBT (poly[N-9''-heptadecanyl-2,7-carbazole-alt-5,5-(4',7'-di-2-thienyl-2',1',3'-benzothiadiazole)]) as a donor and $PC_{71}BM$ ([6,6]-phenyl C_{71}-butyric acid methyl ester) as an acceptor show a power conversion efficiency (PCE) of 6.96%, which is 1.3 times of that of the Al-only device. Most importantly, compared to the reference π-conjugated electrolyte QA-PyBr, DCNQA-PyBr shows much improved electron transport ability and conductivity. As a result, the DCNQA-PyBr based devices only show a slight decrease of electron transport upon increasing the thickness of CIL, thus allow a high PCE with a wide CIL thickness range from 5 nm to 40 nm. Furthermore, introducing DCNQA-PyBr as a CIL into the devices based on P3HT:$PC_{61}BM$ (P3HT = poly(3-hexylthiophene), $PC_{61}BM$ = [6,6]-phenyl C_{61}-butyric acid methyl ester) and PTB7:$PC_{71}BM$ (PTB7 = polythieno[3,4-b]-thiophene-co-benzodithiophene) also leads to significantly enhanced device performance, showing a high PCE of 3.91% and 8.23%, respectively. These results confirm DCNQA-PyBr to be a promising CIL material for solution-processed large-area PSCs.

1. Introduction

Bulk-heterojunction polymer solar cells (PSCs) have drawn tremendous attention due to the unique advantages of low cost, light weight and potential opportunity of fabricating flexible devices by solution processing.[1] Over the past decade, significant progress has been made in rational donor/acceptor structural design,[2] active layer morphology optimization[3] and device interfacial engineering.[4] Power conversion efficiency (PCE) exceed of 10% has been achieved in single-junction PSCs.[5] Alternatively, a great deal of efforts have been invested in solution-processed organic cathode interlayer (CIL) based on π-conjugated polymeric/small-molecular electrolytes.[6] The conventional inorganic CIL materials such as Ca and LiF have already been widely used for a superior device efficiency.[7] However, they are unstable towards oxygen/moisture[8] and are commonly formed by vacuum deposition, which are not suitable for the roll-to-roll process. On the other hand, organic CIL materials can afford simpler device fabrication procedure, better device stability and remarkably improved device performance. Organic CIL materials are commonly composed of a π-conjugated skeleton and several polar groups such as pyridinium, ammonium, sulfonate, and phosphonate. These strong polar ionic groups impart them with proper solubility in polar solvents, allowing solution-processed deposition of water/alcohol solutions. More importantly, large interfacial dipole can be formed between the CIL and the electrode thus efficiently reduces cathode's work function and facilitates electron extraction and transport at the cathode. As a result, the organic CIL can promote high-performance of PSCs due to simultaneously enhanced open-circuit voltage (V_{oc}), short-circuit current (J_{sc}) and fill factor (FF). Up to now, a number of organic CIL materials have been developed with various π-conjugated skeletons,[9-25] such as polyfluorene,[9] polythiophene,[10] porphyrin,[11] metallophthalocyanine,[12] quinacridone[13] etc. Although significantly improved performance have been achieved by incorporating CIL into PSCs, a disadvantage of these CIL materials has been realized, that is, the requirement of ultrathin thickness (commonly less than 10 nm).[21] The thicker CIL leads to charge build-up at the cathode due to poor electron transport abilities and conductivities of the CIL materials mainly due to the *p*-type feature of the π-conjugated backbones. Unfortunately, producing such ultrathin films with high coverage and film homogeneity has been proved to be difficult by large-area roll-to-roll fabrication,[26] which restricts their applicability in future large-area PSCs. Therefore, developing organic CIL materials with good electron transport ability and conductivity is now an urgent issue. In addition, CIL materials based on small molecules are more attractive compared to the polymeric

State Key Laboratory of Supramolecular Structure and Materials, Jilin University, Changchun, Qianjin Avenue, 130012, P.R. China. E-mail: fhli@jlu.edu.cn; yuewang@jlu.edu.cn

† Electronic Supplementary Information (ESI) available: [UV-visible absorption spectra, cyclic voltammograms curves, TGA curves, dark *J-V* curves of the devices, $J^{1/2}$-*V* curves of the electron-only devices, AFM images, and EQE curves]. See DOI: 10.1039/x0xx00000x

competitors due to several advantages such as well-defined structures, simple synthesis and purification methods, and good batch-to-batch reproducibility. In this context, we focus on the development of novel CIL materials based on *n*-type small molecules, which should show much improved electron mobility and conductivity. It is noted that several kinds of these CIL materials have been reported, such as perylene diimide[22a] and fullerene[27] derivatives. They can efficiently work in a wider thickness range in PSCs due to the excellent conductivities. Recently, we have developed a class of dicyanomethylenated quinacridone (DCNQA) derivatives that serve as electron acceptors in PSCs. [28] The incorporation of strong electron-withdrawing dicyanomethylene groups to quinacridone (QA) skeleton endows the resulting DCNQA derivatives with low-lying LUMO (lowest unoccupied molecular orbital) level and good electron transport property. The PSCs using P3HT as a donor and C8-DCNQA as an acceptor showed a PCE of 1.57%. In addition, DCNQA derivatives can be easily synthesized from inexpensive industrial QA pigment.[29] The DCNQA skeleton is expected to be further modified at multiple active sites,[30] thereby provides more structural versatility.

In this contribution, we synthesized a novel *N,N'*-dioctylpyridinium DCNQA derivative, namely DCNQA-PyBr and a reference electrolyte, *N,N'*-dioctylpyridinium quinacridone (QA-PyBr) (Fig. 1a). Two flexible alkyl groups were introduced for better solubility in alcohol and improved film-forming property on active layer.[12b] They were employed as CIL in the PSCs based on PCDTBT (poly[N-9''-heptadecanyl-2,7-carbazole-alt-5,5-(4',7'-di-2-thienyl-2',1',3'-benzothiadiazole)]):$PC_{71}BM$

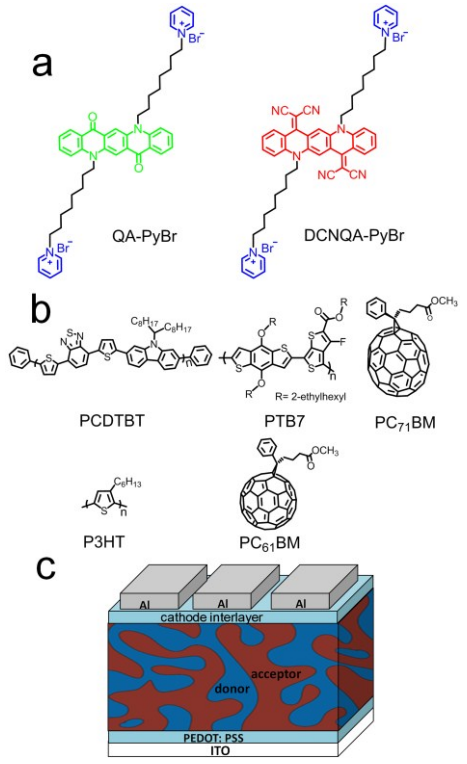

Fig. 1 (a) Molecular structures of the electrolytes QA-PyBr and DCNQA-PyBr. (b) Molecular structures of PCDTBT, PTB7, $PC_{71}BM$, P3HT, and $PC_{61}BM$. (c) Architecture of the device.

([6,6]-phenyl C_{71}-butyric acid methyl ester) as an active layer (Fig. 1b, 1c). Inserting DCNQA-PyBr or QA-PyBr as CIL has significantly improved the PCE of device due to the simultaneously enhanced J_{sc}, V_{oc}, and FF. Furthermore, the high performance can be kept in a wide range of DCNQA-PyBr layer thickness (from 5 nm to 40 nm), which can be attributed to the much improved electron transport ability and higher conductivity of DCNQA-PyBr. On the other hand, the PCE of the QA-PyBr based devices dramatically dropped upon increasing thickness of the QA-PyBr layer. In addition, inserting DCNQA-PyBr as the CIL also led to significant performance improvements of the PSCs based on P3HT:$PC_{61}BM$ (P3HT = poly(3-hexylthiophene), $PC_{61}BM$ = [6,6]-phenyl C_{61}-butyric acid methyl ester) and PTB7:$PC_{71}BM$ (PTB7 = polythieno[3,4-b]-thiophene-co-benzodithiophene), indicating universality of DCNQA-PyBr as CIL for the PSCs.

2. Results and discussion

The DCNQA-based electrolyte DCNQA-PyBr was conveniently synthesized by two steps on gram-scale (Scheme 1). The intermediate DCNQA-Br was synthesized by Knoevenagel condensation between QA-Br and malononitrile. The ionization of DCNQA-Br and QA-Br with pyridine was then performed to afford DCNQA-PyBr, and QA-PyBr as a reference molecule. DCNQA-PyBr and QA-PyBr are well soluble in methanol but insoluble in chlorobenzene and *o*-dichlorobenzene. This orthogonal solubility with respect to the polymers and fullerenes can avoid the damage of the underlying layers and give an opportunity for solution-processed layer-by-layer device. The UV-vis absorption spectra DCNQA-PyBr and QA-PyBr in solution are similar to their neutral analogues C8-DCNQA[28a] and C8-QA[31] (Fig. S1†). Based on the onset reduction potentials, the LUMO energy levels were estimated to be -3.45 eV for DCNQA-PyBr and -3.22 eV

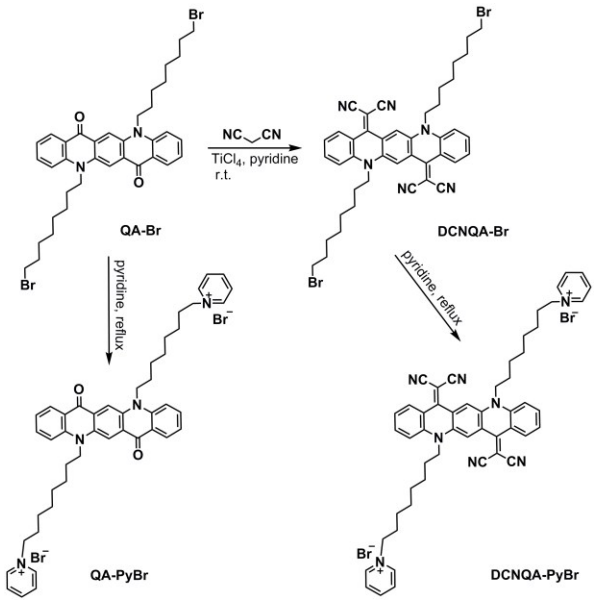

Scheme 1 Synthesis of QA-PyBr and DCNQA-PyBr.

for QA-PyBr (Fig. S2†). The HOMO (highest occupied molecular orbital) level was -5.26 eV for DCNQA-PyBr and -5.46 eV for QA-PyBr by calculation using LUMO energy levels and optical band gaps E_g^{opt} (Table S1†).

To study the effect of introducing DCNQA-PyBr and QA-PyBr as CIL, PSCs were fabricated with a configuration of ITO/PEDOT:PSS/PCDTBT:$PC_{71}BM$/CIL/Al. The two CILs were deposited onto the active layer by spin-coating from their methanol solutions. For comparison, two control devices were also fabricated, that are the Al-only device without the CIL and the methanol-treated device by spin-coating methanol on the active layer. Fig. 2a shows the current density-voltage (*J-V*) characteristics of the devices under the 100 mW cm^{-2} AM. 1.5G irradiation and the performance parameters are summarized in Table 1. More than 20 devices were measured for each configuration and the efficiencies were averaged. The Al-only device gives a maximum PCE of 5.21% with a J_{sc} of 10.24 mA cm^{-2}, a V_{oc} of 0.88 V, and a FF of 57.8%. Incorporating DCNQA-PyBr layer with optimized thickness of 13 nm as the CIL leads to simultaneously enhanced V_{oc} (0.91 V), J_{sc} (11.33 mA cm^{-2}) and FF (67.5%). Overall, the PCE value reached 6.96%, which is 1.3 times of that of the Al-only device. In addition, the device with 4 nm QA-PyBr also exhibited a PCE of 6.70% with J_{sc} of 11.19 mA cm^{-2}, V_{oc} of 0.90 V and FF of 66.4%. The methanol-treated device only exhibited a slightly increase in J_{sc} and V_{oc},

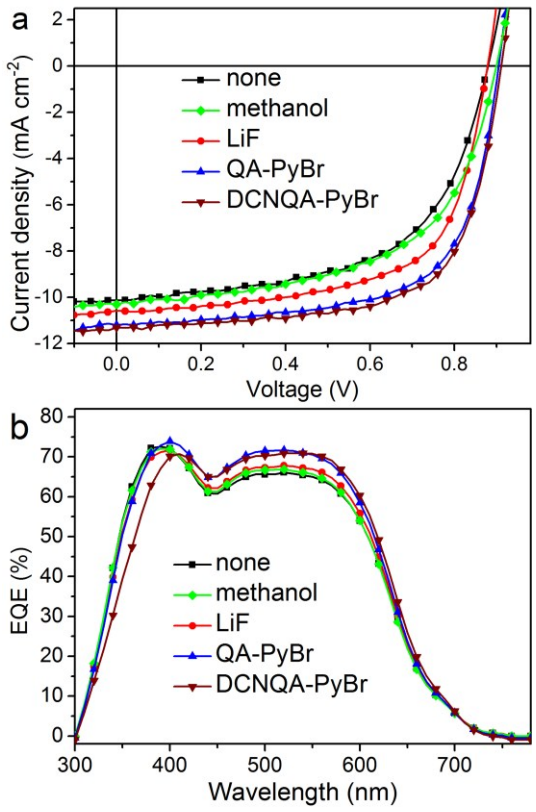

Fig. 2 Effect of QA-PyBr and DCNQA-PyBr interlayers on the performance of devices based on PCDTBT:$PC_{71}BM$. (a) *J-V* characteristics of the QA-PyBr (4 nm), DCNQA-PyBr (13 nm) interlayer incorporated devices, methanol-treated, LiF/Al, and Al-only device measured under 100 mW cm^{-1} AM 1.5G. (b) The external quantum efficiency (EQE) spectra of the Al-only, methanol-treated, LiF, QA-PyBr, and DCNQA-PyBr interlayers inserted devices.

Table 1. Photovoltaic properties of the PCDTBT:$PC_{71}BM$ devices with various interlayers under 100 mW cm^{-2} AM 1.5G irradiation.

CIL	J_{sc} (mA cm^{-2})	V_{oc} (V)	FF (%)	PCE (%)		R_s (Ω cm^2)
				Max	Aver	
none	10.24	0.88	57.8	5.21	5.13	14.4
LiF	10.64	0.88	63.6	5.95	5.89	8.5
methanol	10.30	0.90	57.5	5.33	5.22	12.5
QA-PyBr	11.19	0.90	66.4	6.70	6.56	8.4
DCNQA-PyBr	11.33	0.91	67.5	6.96	6.89	8.0

leading to a PCE of 5.33%. It suggests that the enhanced PCE of the devices with the CIL are mainly contributed by the CIL themselves rather than their solvent (methanol). It's noteworthy that the CIL inserted devices also have superior performance than the conventional LiF/Al based devices (6.96% *vs.* 5.95%) due to the higher J_{sc}, V_{oc} and FF, as shown in Table 1. The average PCE values of the Al-only, LiF/Al, methanol-treated, QA-PyBr and DCNQA-PyBr devices are 5.13%, 5.89%, 5.22%, 6.56% and 6.89% respectively. Fig. 2b shows the external quantum efficiency (EQE) spectra of the corresponding devices. While the methanol-treated device shows similar EQE spectra, the devices with the CIL show higher EQE values than that of the Al-only device in the range of 400 to 600 nm. The J_{sc} values integrated from the EQE spectra agree well to the tested values (Table S2†), indicating that the J_{sc} presented in Fig. 2a are not overvalued.

The increased V_{oc} of the devices with the CIL can be attributed to the lower work functions (WF) of the cathode, which were determined by the ultraviolet photoelectron spectroscopy (UPS) with monochromatized HeI radiation at 21.2 eV (Fig. 3). WF is defined by secondary electron cutoff in the UPS Spectra. The WF values are 4.18 eV and 3.53 eV for bare Al and methanol-treated Al, respectively. QA-PyBr or DCNQA-PyBr coverage provides further lower WF of Al at about 3.30 eV. The reduction of cathode WF can increase the built-in potential across the devices, which influence the internal electric field and give upper limit of the V_{oc}. This was further supported by the increased turn-on voltage deduced from the dark *J-V* curves, which were determined to be 0.99 V, 1.03 V, 1.06 V and 1.04 V for the devices with bare Al, methanol-treated Al, QA-PyBr/Al and DCNQA-PyBr/Al cathodes, respectively (Fig. S4†). These results suggest that introduction of the CIL increases built-in voltage (here considered as the flat-band condition) of the devices, which is responsible for the increase in V_{oc}.

Table 1 shows the series resistances (R_s) of the devices that derived from the slop of the *J-V* curves at V_{oc}. The devices incorporating QA-PyBr and DCNQA-PyBr show R_s of 8.4 Ω cm^2 and 8.0 Ω cm^2, respectively, which are lower than that of the Al-only device (14.4 Ω cm^2). The increase of J_{sc} of the devices with the CIL is attributed to the decrease of resistance.

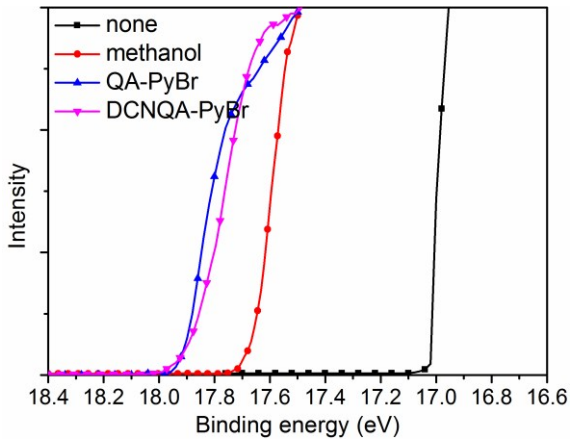

Fig. 3 Ultraviolet photoelectron spectra of bare Al, methanol-treated Al and Al covered by about 3 nm QA-PyBr and DCNQA-PyBr.

Compared to the control devices, the devices incorporating QA-PyBr or DCNQA-PyBr layer show higher FF values, as listed in Table 1. It implies that introduction of the CIL effectively improved charge transport ability. In order to confirm that the electron transport of PSCs is enhanced when QA-PyBr or DCNQA-PyBr is inserted, electron mobility was measured by space charge limited current (SCLC) technique with a device configuration of ITO/Al/PCDTBT:PC_{71}BM/Al or ITO/Al/PCDTBT:PC_{71}BM/CIL/Al. The $J^{1/2}$-V analyses of the electron-only devices are presented in Fig. S5†. The electron mobility in the methanol-treated device (3.4×10^{-4} cm^2 V^{-1} s^{-1}) is almost same to that of the Al-only device (3.6×10^{-4} cm^2 V^{-1} s^{-1}). The electron mobility in the devices with QA-PyBr/Al and DCNQA-PyBr/Al are 9.7×10^{-4} cm^2 V^{-1} s^{-1} and 1.1×10^{-3} cm^2 V^{-1} s^{-1}, respectively. Indeed, the incorporation of a CIL increased the electron mobility, which was in agreement with the increasing trend of FF as listed in Table 1.

Effect of the CIL thickness on the device performance of the devices based on PCDTBT:PC_{71}BM was then investigated. The thickness of QA-PyBr or DCNQA-PyBr was modulated by changing their concentrations from 0.5 mg mL^{-1} to 5.0 mg mL^{-1} (Fig. S6†). The J-V curves of the devices with various thicknesses of CIL are shown in Fig. 4 and the device performance parameters are summarized in Table 2. When QA-PyBr thickness increased from 4 nm to 20 nm, the PCE reduced from 6.70% to 1.71% due to the decrease of J_{sc} (11.19 mA cm^{-2} *vs.* 7.93 mA cm^{-2}) and FF (66.5% *vs.* 23.9%), accompanied by a decline of R_s from 8.4 Ω cm^2 to 221.8 Ω cm^2. The extremely large R_s and the S-shape J-V curve indicate a poor charge transport of the device with 20 nm QA-PyBr, as shown in Fig. 4a. However, the performance of the device with DCNQA-PyBr is less dependent on the CIL thickness, as shown in Fig. 4b. The best PCE (6.96%) was achieved with a 13 nm DCNQA-PyBr layer. Further increasing CIL thickness to 19 nm only leads to a slight drop of J_{sc} and FF, resulting in a PCE of 6.37%, as listed in Table 1. Even when DCNQA-PyBr thickness reached up to 40 nm, the device still demonstrated a PCE of 5.82%, which are much higher than that of the Al-only device. Meanwhile, the R_s slightly increased from 8.0 Ω cm^2 to 11.2 Ω cm^2 when the thickness increased from 5 nm to 40 nm.

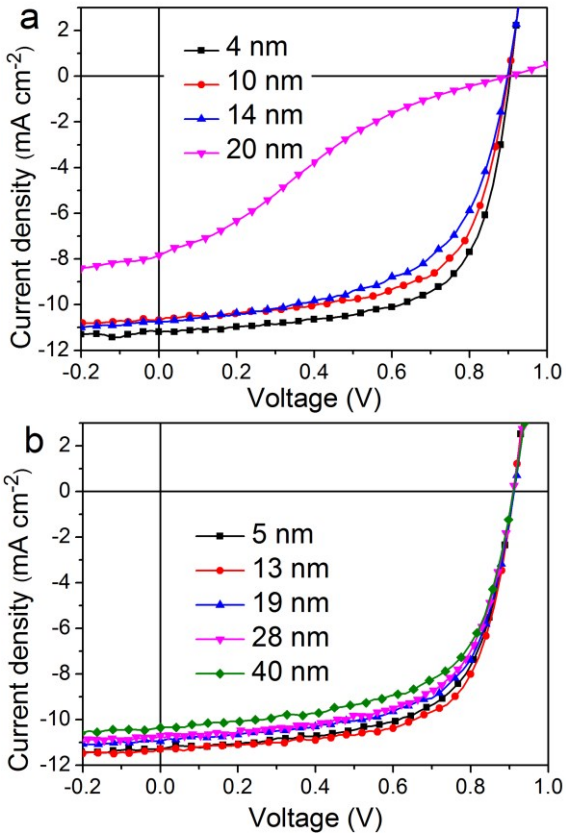

Fig. 4 The effect of the QA-PyBr and DCNQA-PyBr interlayers thickness on the performance of PCDTBT:PC_{71}BM devices. J-V characteristics of the devices with various thicknesses of QA-PyBr (a) and DCNQA-PyBr (b) interlayer.

Table 2. Photovoltaic properties of the devices with various thicknesses of QA-PyBr and DCNQA-PyBr interlayers under 100 mW cm^{-2} AM 1.5G irradiation.

CIL	thickness (nm)	J_{sc} (mA cm^{-2})	V_{oc} (V)	FF (%)	PCE (%)	R_s (Ω cm^2)
QA-PyBr	4	11.19	0.90	66.5	6.70	8.4
	10	10.68	0.90	63.2	6.07	11.0
	14	10.74	0.90	57.6	5.57	12.8
	20	7.93	0.90	23.9	1.71	221.8
DCNQA-PyBr	5	11.28	0.91	64.7	6.64	10.3
	13	11.33	0.91	67.5	6.96	8.0
	19	10.95	0.91	64.0	6.37	10.6
	28	10.70	0.91	63.2	6.15	11.0
	40	10.35	0.91	61.8	5.82	11.2

To elucidate the big difference of the devices performance with DCNQA-PyBr and QA-PyBr based CIL, the electron transport of PSCs with various thicknesses were characterized by J-V measurements of the electron-only devices with a configuration of ITO/Al/PCDTBT:PC_{71}BM/CIL/Al. Fig. 5 presents the J-V characteristics of the electron-only devices with the QA-PyBr (a) and DCNQA-PyBr (b) layer. Upon increasing the

thickness of the QA-PyBr layer to 20 nm, the device exhibits one order of magnitude decrease of current density. However the current densities of the devices with DCNQA-PyBr are independent on the CIL thickness. Even when the thickness of DCNQA-PyBr is 40 nm, the device only shows a slight decline of current density (Fig. 5b). These findings indicate that DCNQA-PyBr has much better electron transport ability than QA-PyBr. Furthermore, the conductivity measurements (Fig. 6) have demonstrated that DCNQA-PyBr has a higher conductivity (2.25×10^{-6} S cm^{-1}) than that of the QA-PyBr (1.23×10^{-7} S cm^{-1}). Therefore, we infer that the high efficiency of the PSCs with thick DCNQA-PyBr interlayer (10-40 nm) is originated from its improved electron transport ability and higher conductivity.

Good film formation atop the hydrophobic active layer is a fundamental requirement for solution-processed CIL materials. The film morphologies of the DCNQA-PyBr layers on PCDTBT:$PC_{71}BM$ were investigated by atomic force microscopy (AFM). The PCDTBT:$PC_{71}BM$ layer has a smooth surface with root-mean-square (RMS) roughness of 0.56 nm (Fig. 7a). The 5 nm DCNQA-PyBr film spin-coated on the active layer is rather rough (RMS = 2.74 nm) due to its self-aggregation (Fig. 7b). The rough morphology of this ultrathin film is unfavourable for the device performance due to non-uniform coverage of the active layer. Surprisingly, much improved morphologies were formed for the thicker DCNQA-PyBr films. They show smoother films with RMS smaller than 1 nm (13 nm film: RMS = 0.69 nm, 19 nm film: RMS = 0.71 nm, 28 nm film: RMS = 0.60 nm), though some visible islands still existed (Fig. 7c-e). The 40 nm DCNQA-PyBr film shows a smoother and more homogeneous surface with a low RMS of 0.31 nm (Fig. 7f). Therefore, a uniform DCNQA-PyBr film atop of the active layer can be obtained in a wide range of thickness. Furthermore, the QA-PyBr films atop the active layer are smooth and even more uniform than those of the DCNQA-PyBr (Fig. S8†), indicating that the different device performances stem from the distinct electron transport

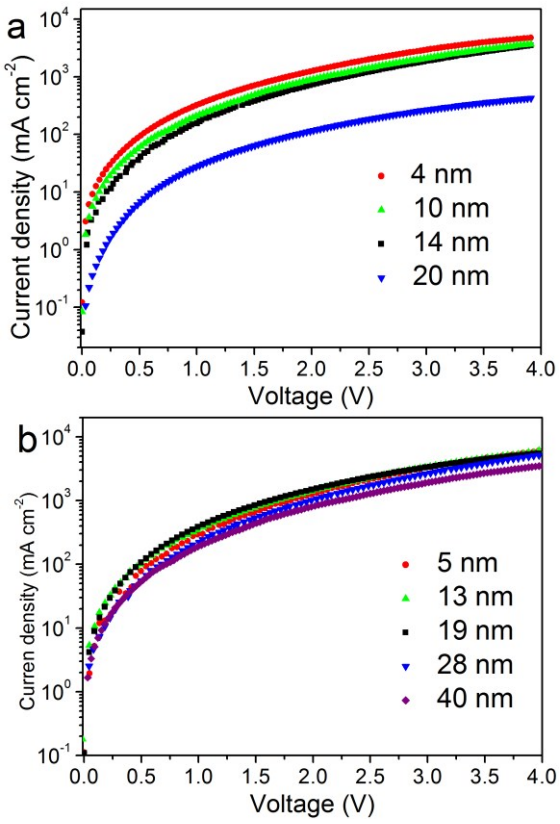

Fig. 5 *J-V* characteristics of the electron-only devices with an active layer of PCDTBT:$PC_{71}BM$ and various thicknesses of QA-PyBr (a) and DCNQA-PyBr (b) interlayers.

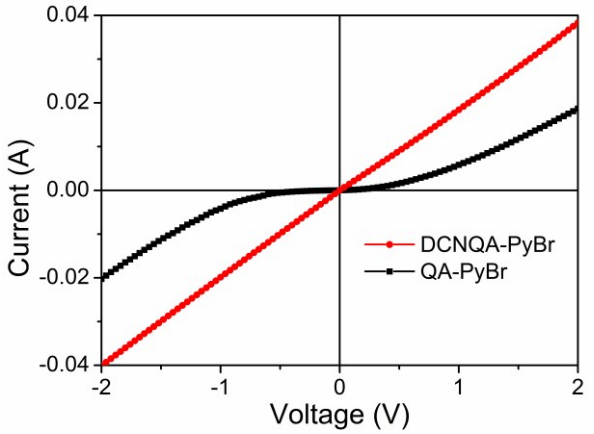

Fig. 6 *I-V* curves of the conductivity measurements of DCNQA-PyBr and QA-PyBr with a configuration of ITO/DCNQA-PyBr (QA-PyBr)/Al. The conductivities were calculated from Ohm's law at the linear regions.

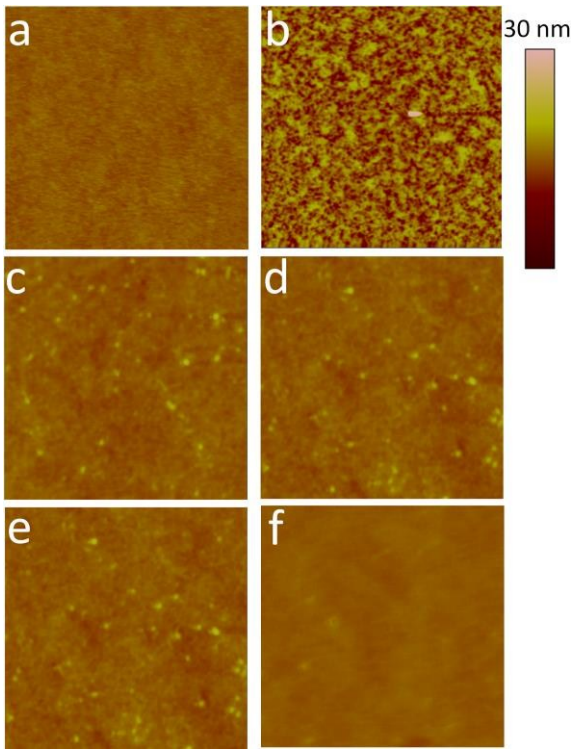

Fig. 7 Atomic force microscopy (AFM) images (5 × 5 μm) of (a) PCDTBT:$PC_{71}BM$ layer and (b-f) various thicknesses DCNQA-PyBr interlayers atop of the PCDTBT:$PC_{71}BM$ layer. (b) 5 nm, RMS: 2.74 nm; (c) 13 nm, RMS: 0.69 nm; (d) 19 nm, RMS: 0.71 nm; (e) 28 nm, RMS: 0.60 nm; (f) 40 nm, RMS: 0.31 nm.

ability and conductivity of these CIL materials rather than their different film forming abilities.

Inspired by these outstanding properties of DCNQA-PyBr, we further checked its performance in P3HT:$PC_{61}BM$ and PTB7:$PC_{71}BM$ based devices. The CIL with an optimized thickness of 13 nm was employed. The *J-V* characteristics of the devices under 100 mW cm^{-2} AM 1.5G irradiation are presented in Fig. 8a and 8b, and the performance parameters are summarized in Table 3. As we expected, for the P3HT:$PC_{61}BM$ system, the CIL-inserted device shows enhanced J_{sc} from 9.12 mA cm^{-2} (device I) to 10.25 mA cm^{-2} (device III), V_{oc} from 0.51 V to 0.61 V, FF from 51.8% to 62.5% and PCE from 2.41% to 3.91%. Meanwhile, the R_s of the devices reduced from 14.8 Ω cm^2 to 9.1 Ω cm^2. Similarly, for the PTB7:$PC_{71}BM$ devices, inserting DCNQA-PyBr as CIL led to enhanced J_{sc} from 14.62 mA cm^{-2} (device IV) to 16.51 mA cm^{-2} (device VI), V_{oc} from 0.67 V to 0.74 V and FF from 54.0% to 67.3%. Overall, a high PCE of 8.23% was obtained, which are more than 1.5 times higher than that of the Al-only device. The R_s of the devices reduced from 13.2 Ω cm^2 to 5.2 Ω cm^2. These results demonstrate the universality of DCNQA-PyBr based CIL for PSCs with different photoactive layers. The DCNQA-PyBr inserted devices also have higher PCE values than those of the conventional LiF/Al cathode for P3HT:$PC_{61}BM$ and PTB7:$PC_{71}BM$ systems (Table 3). The EQE spectra of the devices are shown in Fig. 9. The J_{sc} values integrated from the EQE spectra agree well to the tested values (Table S3† and S4†).

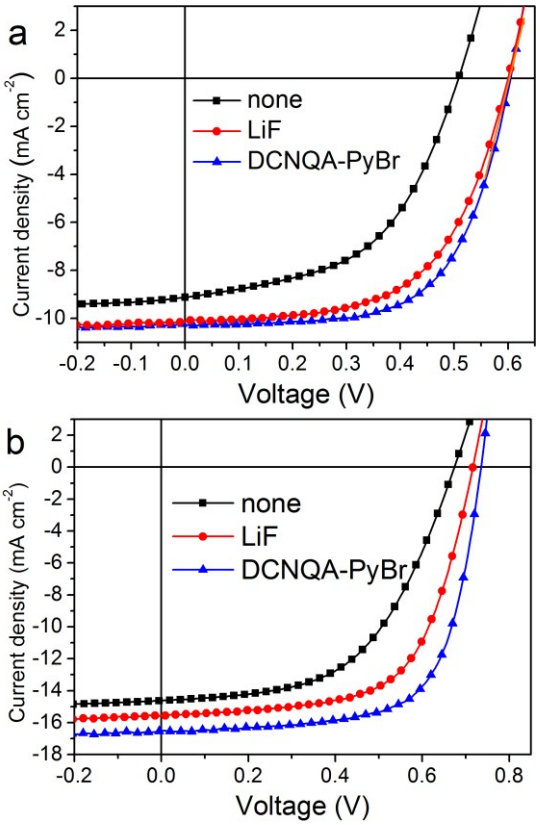

Fig. 8 The effect of DCNQA-PyBr interlayer on the performance of (a) P3HT:$PC_{61}BM$ and (b) PTB7:$PC_{71}BM$ devices. Current density-voltage (*J-V*) characteristics of the Al-only, LiF/Al and devices with DCNQA-PyBr interlayer.

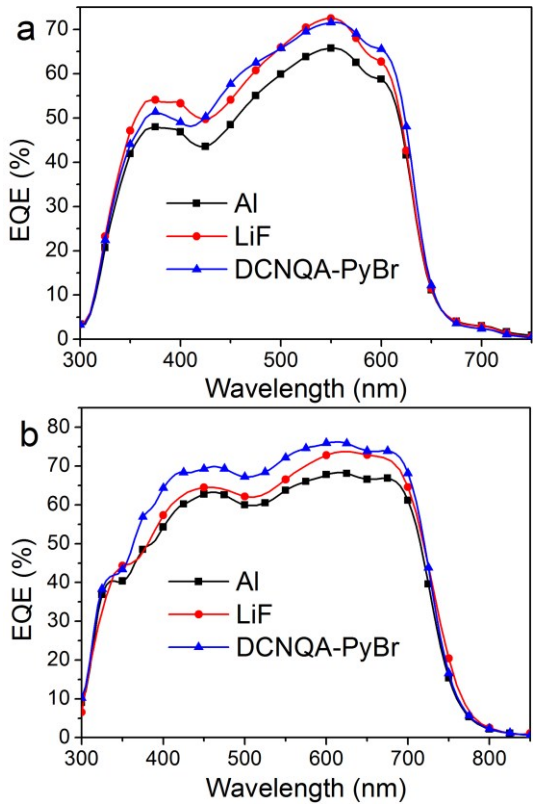

Fig. 9 The EQE spectra of the Al-only, LiF/Al, and DCNQA-PyBr interlayers inserted devices for (a) P3HT:$PC_{61}BM$ system and (b) PTB7:$PC_{71}BM$ system.

Table 3. Photovoltaic properties of the P3HT:$PC_{61}BM$ and PTB7:$PC_{71}BM$ based devices with various cathodes under 100 mW cm^{-2} AM 1.5G irradiation.

Device	J_{sc} (mA cm^{-2})	V_{oc} (V)	FF (%)	PCE (%)		*Rs* (Ω cm^2)
				Max	Aver	
I	9.12	0.51	51.8	2.41	2.35	14.8
II	10.13	0.60	58.2	3.54	3.43	11.0
III	10.25	0.61	62.5	3.91	3.87	9.1
IV	14.62	0.67	54.0	5.29	5.25	13.2
V	15.19	0.72	64.3	7.03	6.95	7.3
VI	16.51	0.74	67.3	8.23	8.12	5.2

[a] Device I: ITO/PEDOT:PSS/P3HT:$PC_{61}BM$/Al, device II: ITO/PEDOT:PSS/P3HT:$PC_{61}BM$/LiF/Al, device III: ITO/PEDOT:PSS/P3HT:$PC_{61}BM$/DCNQA-PyBr/Al, device IV: ITO/PEDOT:PSS/PTB7:$PC_{71}BM$/Al, device V: ITO/PEDOT:PSS/PTB7:$PC_{71}BM$/LiF/Al, device VI: ITO/PEDOT:PSS/PTB7:$PC_{71}BM$/DCNQA-PyBr/Al.

3. Conclusions

In summary, a novel n-type π-conjugated electrolyte DCNQA-PyBr was developed and employed as cathode interlayer in PSCs. The incorporation of DCNQA-PyBr as CIL leads to simultaneously improved J_{sc}, V_{oc}, and FF. High PCE values of 6.96%, 3.91%, and 8.23% have been achieved for PSCs with PCDTBT:$PC_{71}BM$, P3HT:$PC_{61}BM$, and PTB7:$PC_{71}BM$ as active layer, respectively, which are much higher than those of the

corresponding Al-only devices. More importantly, DCNQA-PyBr exhibits excellent electron transport property and conductivity, allowing the device work well in a wide range of DCNQA-PyBr interlayer thickness. For PCDTBT:$PC_{71}BM$ based device, a PCE of 5.82% was achieved even when thickness of the DCNQA-PyBr interlayer reached up to 40 nm. On the other hand, the reference CIL material QA-PyBr shows poor electron transport ability and low conductivity. The performance of the QA-PyBr based device is sensitive to the thickness of the CIL. The PCE dropped to 1.71% when thickness of QA-PyBr interlayer reached 20 nm. With the good electron transport ability, facile synthesis and purification, and good film formation ability, DCNQA-PyBr has promising application as low-cost and eco-friendly cathode interlayer in large-area PSCs.

4. Experimental Section

4.1 Synthesis and Characterization

^{1}H NMR and ^{13}C NMR spectra were recorded by Bruker Avance 500 MHz spectrometer with tetramethylsilane (TMS) as the internal standard. Elemental analyses were performed on a Vario Micro (Elementar) spectrometer. Thermogravimetric analyses (TGA) were performed on a TAQ500 thermogravimeter at a heating rate of 10 ℃ min^{-1} under nitrogen. UV-visible absorption spectra were recorded on a Shimadzu UV-2550 spectrophotometer. Cyclic voltammetries were performed on a BAS 100W instrument with a scan rate of 100 mV s^{-1}. A three-electrode configuration was used for the measurement: a platinum electrode as the working electrode, a platinum wire as the counter electrode and an Ag/Ag^+ electrode as the reference electrode. A 0.1 M solution of tetrabutylammonium hexafluorophosphate (TBAPF) in DMF was used as the supporting electrolyte.

Dichloromethane (CH_2Cl_2) and pyridine were distilled over CaH_2 and KOH, respectively. The other reagents were purchased from Sigma-Aldrich Chemical Co. and directly used without purification. All reactions were performed under a N_2 atmosphere. *N*,*N*'-bis(8-bromooctyl)-quinacridone (**QA-Br**) was prepared by the alkylation of quinacridone with 1,8-dibromooctane according to our reported procedure.[32] The synthesis and characterization of QA-PyBr and DCNQA-PyBr are presented as follows.

DCNQA-Br. To a 500 mL two-neck flask, **QA-Br** (1.74g, 2.50 mmol) and malononitrile (0.33g, 5.00 mmol) were dissolved in 300 mL dry CH_2Cl_2. $TiCl_4$ (14.25 g, 75.0 mmol) was slowly added via dropping funnel at 10 ℃. After vigorously stirring for 10 minutes, pyridine (31.60 g, 400.0 mmol) was slowly added via dropping funnel. Then the mixture was stirring for 24 hours at room temperature. The solvent and the residual pyridine were evaporated under reduced pressure. The product was obtained as dark blue solid after purified by silica gel chromatography using CH_2Cl_2 as eluent (1.34 g, 68%). ^{1}H NMR (500 MHz, $CDCl_3$): δ 8.62 (s, 2H), 8.58 (dd, J^1 = 8.0 Hz, J^2 = 1.0 Hz, 2H), 7.80-7.77 (m, 2H), 7.52 (d, *J* = 3.5 Hz, 2H), 7.38 (t, *J* = 7.5 Hz, 2H), 4.48 (t, *J* = 8.0 Hz, 4H), 3.48 (t, *J* = 7.0 Hz, 4H), 2.10-2.03 (m, 4H), 1.96-1.90 (m, 4H), 1.70-1.64 (m, 4H), 1.58-1.43 (m, 12H). ^{13}C NMR (125 MHz, $CDCl_3$): δ 155.07, 139.26, 134.45, 133.61, 127.26, 122.83, 122.00, 117.60, 117.16, 116.76, 114.48, 111.62, 70.29, 49.17, 34.00, 32.70, 29.08, 28.66, 27.98, 27.03, 26.69.

QA-PyBr. QA-Br (1.74 g, 2.50 mmol) was dissolved in 100 mL pyridine and the mixture was refluxed overnight. After cooling to room temperature, the solid was filtered out and washed by 100 mL CH_2Cl_2. The product was obtained as red solid (1.85 g, 85%). ^{1}H NMR (500 MHz, CD_3OD): δ 9.10 (d, *J* = 5.5 Hz, 4H), 8.63 (t, *J* = 7.5 Hz, 2H), 8.38 (s, 2H), 8.26 (dd, *J* = 8.0 Hz, *J* = 1.5 Hz, 2H), 8.16 (t, *J* = 7.5 Hz, 4H), 7.68-7.65(m, 2H), 7.48 (d, *J* = 9.0 Hz, 2H), 7.15 (t, *J* = 7.5 Hz, 2H), 4.73 (t, *J* = 7.5 Hz, 4H), 4.34 (t, *J* = 8.0 Hz, 4H), 2.14-2.10 (br, 4H), 1.89-1.83 (br, 4H), 1.63-1.51 (br, 16H). ^{13}C NMR (125 MHz, CD_3OD): δ 177.79, 145.48, 144.61, 141.86, 134.92, 134.80, 128.15, 126.87, 125.33, 120.80, 120.16, 115.00, 112.86, 61.73, 45.84, 31.02, 28.60, 28.50, 26.39, 26.11, 25.65. Anal. Calcd for $C_{42}H_{42}Br_2N_6$: C 63.80, H 5.35, N 10.63, Found: C 64.02, H 5.31, N 10.58.

DCNQA-PyBr. The synthesis procedure was as same as that of **QA-PyBr**. The product was obtained as dark blue solid with 81% yield. ^{1}H NMR (500 MHz, CD_3OD): δ 9.06 (d, *J* = 5.0 Hz, 4H), 8.63 (m, 4H), 8.49 (d, *J* = 8.0 Hz, 2H), 8.17 (m, 4H), 7.78 (t, *J* = 7.5 Hz, 2H), 7.69 (d, *J* = 8.0 Hz, 2H), 7.31 (t, *J* = 7.5 Hz, 2H), 4.70 (t, *J* = 7.0 Hz, 4H), 4.49 (t, *J* = 7.0 Hz, 4H), 2.10-1.99 (m, 8H), 1.59-1.49 (m, 16H). ^{13}C NMR (125 MHz, CD_3OD): δ 154.93, 145.51, 144.55, 139.15, 134.45, 133.38, 128.18, 126.61, 122.61, 121.53, 118.98 117.68, 116.84, 115.05, 111.74, 68.87, 61.76, 48.37, 30.98, 28.56, 28.45, 26.61, 26.10, 25.58. Anal. Calcd for $C_{52}H_{52}Br_2N_8$: C 65.82, H 5.52, N 11.81, Found: C 63.79, H 5.54, N 11.39.

4.2 Device Fabrication and Characterization

P3HT was purchased from Rieke Metals (USA). PCDTBT and PTB7 were purchased from 1-material Chemscitech Inc. (Canada). $PC_{71}BM$ and $PC_{61}BM$ were purchased from American Dye Source (USA). The ITO-coated glass was pre-cleaned and treated with plasma for 5 min. A 35 nm PEDOT: PSS (Baytron PVP Al 4083) layer was spin coated and baked at 120℃ for 10 min. The device was then transferred to a nitrogen glove box. For PCDTBT:$PC_{71}BM$ devices, a blend of 7 mg PCDTBT and 28 mg $PC_{71}BM$ was dissolved into 1 mL mixed solvent (chlorobenzene: *o*-dichlorobenzene = 1: 3, v/v) and stirred overnight. The solution was spin-coated onto the substrate at 2000 rpm for 40 s and then annealed at 75 ℃ for 10 min. The thickness of the active layer was *ca.* 90 nm; For P3HT:$PC_{61}BM$ device, a blend of 17 mg P3HT and 17 mg $PC_{61}BM$ was dissolved into 1 mL of *o*-dichlorobenzene and stirred for 2 days. The solution was spin-coated onto the substrate at 600 rpm for 40 s, followed by solvent annealing at room temperature for 2 h, and thermally annealing at 110 ℃ for 10 min to produce an active layer with a thickness of 180 nm; The PTB7:$PC_{71}BM$ active layer was formed by spin-coating the chlorobenzene: DIO (1, 8-diiodoctane) (v: v = 97: 3) solution (containing 10 mg mL^{-1} PTB7 and 15 mg mL^{-1} $PC_{71}BM$) at 1000 rpm for 60 s. The residual DIO was removed in vacuum overnight. The thickness of the active layer was *ca.* 120 nm.

The QA-PyBr or DCNQA-PyBr cathode interlayer was subsequently deposited on the active layer from the methanol solution. The thickness was regulated by varying the concentrations from 0.5 to 5.0 mg mL^{-1}. Finally, 100 nm Al was thermal-deposited under pressure of 2×10^{-6} mbar. The active area of each pixel was 2×2 mm^2. The control device without interlayer was fabricated under the same condition. Photovoltaic performance of the device was tested under 1 sun, AM 1.5 full spectrum solar simulator (Photo Emission Tech. Inc.) with an irradiation intensity of 100 mW cm^{-2} calibrated with a standard silicon solar cell traced to the National institute of metrology, China. The current-voltage (*J-V*) characteristics under light and in dark were measured by using a Keithley 2400 source meter. External quantum efficiency (EQE) spectra were measured using Q Test Station 2000 (Crowntech Inc. USA) under ambient condition. AFM (by Burker Dimension ICON) was carried out directly on the surface of the fabricated devices in the PeakForce QNM mode under ambient condition. The AFM images and RMS values were drawn and calculated by the software NanoScope Analysis. The thickness of the 20 nm QA-PyBr and 40 nm DCNQA-PyBr films were determined by a profilometer (DEKTAK 150). The data were averaged from 5 films. The thickness of the other films was estimated by an absorbance-thickness curve (Fig. S6†) that assumed the thickness is linear dependent on maximum absorbance.

The electron mobility of the devices was measured by the SCLC (space charge limited current) method. The device structure is ITO/Al/PCDTBT:$PC_{71}BM$/QA-PyBr (DCNQA-PyBr)/Al. The mobility is calculated by the following equation:

$$\mu = \frac{8d^3}{9\varepsilon_0\varepsilon_r}\left(\frac{\sqrt{J}}{V}\right)^2$$

where J is the current density, ε_r is the dielectric constant of the material (assumed to be 3.9), ε_o is the vacuum permittivity (8.8542×10^{-12} F m^{-1}), d is the film thickness and V is the voltage drop across the device, $V = V_{app} - V_r - V_{bi}$. V_r (the voltage drop due to contact resistance and series resistance across the electrodes) and V_{bi} (the built-in voltage of the device due to the difference in work function of the electrodes at both sides of the active layer) are subtracted from experimental applied voltage. A straight line going through the origin of $J^{1/2}$-V curves for the devices signifies that the mobility is field independent at field up to 2×10^5 V cm^{-1}.

The conductivities of QA-PyBr and DCNQA-PyBr were measured with a device configuration of ITO/QA-PyBr (DCNQA-PyBr)/Al. The film thickness of QA-PyBr and DCNQA-PyBr was ca. 50 nm and the active area was 2×2 mm^2. The *I-V* plots were measured by using a Keithley 2400 source meter. The conductivities were calculated from Ohm's law at the linear voltage regions.

Acknowledgements

This work was supported by grants from the National Basic Research Program of China (2014CB643500) and Natural Science Foundation of China (51173065, 51273077).

Notes and references

1 (a) G. Li, R. Zhu and Y. Yang, *Nat. Photonics.*, 2012, **6**, 153; (b) L. Dou, J. You, J. Yang, C. C. Chen, Y. He, S. Murase, T. Moriarty, K. Emery, G. Li and Y. Yang, *Nat. Photonics*., 2012, **6**, 180.

2 (a) Y. J. Cheng, S. H. Yang and C. S. Hsu, *Chem. Rev.*, 2009, **109**, 5868; (b) J. Chen and Y. Cao, *Acc. Chem. Res.*, 2009, **42**, 1709; (c) M. Zhang, X. Guo, W. Ma, H. Ade and J. H. Hou, *Adv. Mater.,* 2015, **27**, 4655; (d) Z. G. Zhang and Y. F. Li, *Sci. China Chem.,* 2015, **58**, 192.

3 (a) J. S. Moon, J. Jo and A. J. Heefer, *Adv, Energy Mater.,* 2012, **2**, 304; (b) M. T. Dang, L. Hirsch, G. Wantz and J . D. Wuest, *Chem. Rev.,* 2013, **113**, 3734.

4 (a) H. Wu, *Sci. China Chem.,* 2015, **58**, 189; (b) W. Cao and J. Xue, *Energy Environ. Sci.,* 2014, **7**, 2123; (c) C. Gu, Y. Chen, Z. Zhang, S. Xue, S. Sun, K. Zhang, C. Zhong, H. Zhang, Y. Pan, Y. Lv, Y. Yang, F. Li, S. Zhang, F. Huang and Y. Ma, *Adv. Mater.,* 2013, **25**, 3443; (d) C. E. Small, S. Chen, J. Subbiah, C. M. Amb, S.-W. Tsang, T.-H. Lai, J. R. Reynolds and F. So, *Nat. Photonics*, 2012, **6**, 115.

5 (a) T. Liu, J. Zhao, Z, Li, C. Mu, W. Ma, H. Hu, K. Jiang, H. Lin, H. Ade and H. Yan, *Nat. Commun.,* 2014, 5293; (b) V. Vohra, K. Kawashima, T. Kakara, T. Koganezawa, I. Osaka, T. Takimiya and H. Murata, *Nat. Photonics* 2015, **9**, 403; (c) S. Zhang, L. Ye, W. Zhao, B. Yang, Q. Wang and J. H. Hou, *Sci. China Chem.,* 2015, **58**, 248; (d) F. Huang, *Sci. China Chem.,* 2015, **58**, 190.

6 (a) Z. Hu, K. Zhang, F. Huang and Y. Cao, *Chem. Commun.*, 2015, **51**, 5572; (b) Z. He, H. B. Wu and Y. Cao, *Adv. Mater.,* 2014, **26**, 1006; (c) C. Duan, K. Zhang, C. Zhong, F. Huang and Y. Cao, *Chem. Soc. Rev.*, 2013, **42**, 9071; (d) C. C. Cheuh, C.-Z. Li and A. K. Y. Jen, *Energy Environ. Sci.*, 2015, **8**, 1160.

7 (a) S. Chen, J. R. Manders, S. W. Tsang and F. So, *J. Mater. Chem.*, 2012, **22**, 24202; (b) H. L. Yip and A. K. Y. Jen, *Energy Environ. Sci.*, 2012, **5**, 5994; (c) R. Steim, F. R. Kogler and C. J. Brabec, *J. Mater. Chem.*, 2010, **20**, 2499; (d) L. M. Chen, Z. Xu, Z. Hong and Y. Yang, *J. Mater. Chem.*, 2010, **20**, 2575.

8 (a) M. Jorgensen, K. Norrman, S. A. Gevorgyan, T. Tromholt, B. Andreasen and F. C. Krebs, *Adv. Mater.,* 2012, **24**, 580; (b) M. Jorgensen, K. Norrman and F. C. Krebs, *Sol. Energy Mater. Sol. Cells,* 2008, **92**, 686.

9 (a) S. J. Liu, K. Zhang, J. M. Lu, J. Zhang, H.-L. Yip, F. Huang and Y. Cao, *J. Am. Chem. Soc.*, 2013, **135**, 15326; (b) Z. He, C. Zhong, S. Su, M. Xu, H. Wu and Y. Cao, *Nat. Photonics*, 2012, **6**, 591; (c) Z. He, C. Zhong, X. Huang, W.-Y. Wong, H. Wu, L. Chen, S. Su and Y. Cao, *Adv. Mater.*, 2011, **23**, 4636; (d) Y. Zhao, Z. Y. Xie, C. J. Qin, Y. Qu, Y. H. Geng and L. W. Wang, *Energy Mater. Sol. Cells*, 2009, **93**, 604; (e) B. Xu, Z. Zheng, K. Zhao and J. H. Hou, *Adv. Mater.*, 2015, DOI: 10.1002/adma.201502989.

10 (a) Y.-M. Chang, R. Zhu, E. Richard, C.-C. Chen, G. Li and Y. Yang, *Adv. Funct. Mater.*, 2012, **22**, 3284; (b) J. H. Seo, A. Gutacker, Y. Sun, H. Wu, F. Huang, Y. Cao, U. Scherf, A. J. Heeger and G. C. Bazan, *J. Am. Chem. Soc.*, 2011, **133**, 8416.

11 (a) T. Jia, W. L. Zhou, F. H. Li, Y. J. Gao, L. Wang, J. X. Han, J. Y. Zhang and Y. Wang, *Sci. China Chem.,* 2015, **58**, 323; (b) M. Vasilopoulou, D. G. Georgiadou, A. M. Douvas, A. Soultati, V. Constantoudis, D. Davazoglou, S. Gardelis, L. C. Palilis, M. Fakis, S. Kennou, T. Lazarides, A. G. Coutsolelos and P. Argitis, *J. Mater. Chem. A,* 2014, **2**, 182.

12 (a) X. Cheng, S. H. Sun, Y. C. Chen, Y. J. Gao, L. Ai, T. Jia, F. H. Li and Y. Wang, *J. Mater. Chem. A*, 2014, **2**, 12484; (b) T. Jia,

W. L. Zhou, Y. C. Chen, J. X. Han, L. Wang, F. H. Li and Y. Wang, *J. Mater. Chem. A*, 2015, **3**, 4547; (c) T. Jia, J. X. Han, W. L. Zhou, L. Wang, M. Wu, W. Chen, Y. C. Chen, F. H. Li and Y. Wang, *Sol. Energy Mater. Sol. Cells*, 2015, **141**, 93.

13 T. V. Pho, H. Kim, J. H. Seo, A. J. Heeger and F. Wudl, *Adv. Funct. Mater.*, 2011, **21**, 4338.

14 K. Zhang, Z. C. Hu, R. G. Xu, X.-Fang, Jiang, H.-L. Yip, F. Huang and Y. Cao, *Adv. Mater.*, 2015, **27**, 3607.

15 S. Y. Yao, P. F. Li, J. Bian, Q. F. Dong, C. Im and W. J. Tian, *J. Mater. Chem. A,* 2013, **1**, 11443.

16 R. Q. Yang, Y. H. Xu, X. D. Dang, T. Q. Nguyen, Y. Cao and G. C. Bazan, *J. Am. Chem. Soc.,* 2008, **130**, 3282.

17 H. P. Xiao, J. S. Miao, J. Q. Cao, W. Yang, H. B. Wu and Y. Cao, *Org. Electron.*, 2014, **15**, 758

18 D. C. Chen, H. Zhou, M. Liu, W. M. Zhao, S. J. Su and Y. Cao, *Macromol. Rapid Commun.,* 2013, **34**, 595.

19 H. Ye, X. Hu, Z. Jiang, D. Chen, X. Liu, H. Nie, S. J. Su, X. Gong and Y. Cao, *J. Mater. Chem. A*, 2013, **1**, 3387.

20 (a) S. S. Li, M. Lei, M. L. Lv, S. E. Watkins, Z. A. Tan, J. Zhu, J. H. Hou, X. W. Chen and Y. F. Li, *Adv. Energy Mater.*, 2013, **3**, 1569; (b) Q. Mei, C. Li, X. Gong, H. Lu, E. Jin, C. Du, Z. Lu, L. Jiang, X. Meng, C. Wang and Z. Bo, *ACS Appl. Mat. Interfaces,* 2013, **5**, 8076; (c) Z. G. Zhang, H. Li, B. Qi, D. Chi, Z. Jin, Z. Qi, J. Hou, Y. Li and J. Wang, *J. Mater. Chem. A,* 2013, **1**, 9624; (d) X. Li, W. Zhang, Y. Wu, C. Mina and J. Fang, *J. Mater. Chem. A*, 2013, **1**, 12413

21 S. J. Liu, K. Zhang, J. M. Lu, J. Zhang, H. L. Yip, F. Huang and Y. Cao, *J. Am. Chem. Soc.,* 2013, **135**, 15326.

22 (a) Z.-G. Zhang, B. Qi, Z. Jin, D. Chi, Z. Qi, Y. F. Li and J. Wang, *Energy Environ. Sci.*, 2014, **7**, 1966; (b) Y. Liu, Z. A. Page, T. P. Russell and T. Emrick, *Angew. Chem. Int. Ed.,* 2015, **54**, 11485.

23 (a) D. Chen, H. Zhou, M. Liu, W.-M. Zhao, S. J. Su and Y. Cao, *Macromol. Rapid Commun.*, 2013, **34**, 595; (b) L. Hu, C. Li, A. Hu, X, Hu, Y. Zhang, L. Chen and Y. Chen, *Macromolecules,* 2015, **48**, 5578.

24 T. H. Reilly, A. W. Hains, H.-Y. Chen and B. A. Gregg, *Adv. Energy Mater.*, 2012, **2**, 455.

25 K. Sun, B. Zhao, V. Murugesan, A. Kumar, K. Zeng, J. Subbiah, W. W. H. Wong, D. J. Jones and J. Ouyang, *J. Mater. Chem.*, 2012, **22**, 24155.

26 F. C. Krebs, *Sol. Energy Mater. Sol. Cells*, 2009, **93**, 465.

27 (a) Z. A. Page, Y. Liu, V. V. Duzhko, T. P. Russell and T. Emrick, *Science*, 2014, **346**, 441; (b) C.-Z. Li, C.-Y. Chang, Y. Zang, H.-X. Ju, C.-C. Chueh, P.-W. Liang, N, Cho, D. S. Ginger and A. K.-Y. Jen, *Adv. Mater.*, 2014, **26**, 6262.

28 (a) T. Zhou, T. Jia, B. Kang, F. H. Li, M. Fahlman and Y. Wang, *Adv. Energy Mater.*, 2011, **1**, 431; (b) C. Wang, W. Chen, S. Chen, S. Zhao, J. Zhang, D. Qiu and Y. Wang, *New J. Chem.*, 2012, **36**, 1788.

29 (a) E. B. Faulkner and R. J. Schwartz, *High Performance Pigments*, Wiley-VCH, Wienheim, 2009; (b) G. Lincke, *Dyes Pigm.*, 2002, **52**, 169; (c) S. S. Labana and L. L. Labana, *Chem. Rev.*, 1967, **67**, 1.

30 (a) G. Lincke, *Dyes Pigm.*, 2002, **52**, 169; (b) J. J.-A. Chen, T. L. Chen, B. S. Kim, D. A. Poulsen, J. L. Mynar, J. M. J. Fréchet and B. W. Ma, *ACS Appl. Mater. Interfaces*, 2010, **2**, 2679; (b) I. Javed, Z. Zhang, T. Peng, T. Zhou, H. Zhang, M. I. Khan, Y. Liu and Y. Wang, *Sol. Energy Mater. Sol. Cells*, 2011, **95**, 2670; (c) C. Wang, D. Chen, W. Chen, S. Chen, K. Ye, H. Zhang, J. Zhang and Y. Wang, *J. Mater. Chem. C*, 2013, **1**, 5548.

31 C. Wang, K. Wang, Q, Fu, J. Zhang, D. Ma and Y. Wang, *J. Mater. Chem. C*, 2013, **1**, 410.

32 C. Dou, D. Li, H. Gao, C. Wang, H. Zhang and Y. Wang, *Langmuir*, 2010, **26**, 2113.

N-type cathode interlayer with a wide thickness range in high-performance polymer solar cells due to its good electron transport ability and high conductivity.